GROUND EFFECT CALCULATION OF WING-TAIL CONFIGURATIONS WITH NON-LINEAR BEHAVIOR

Paulo H. Iscold Andrade de Oliveira, iscold@ufmg.br
Luiz Augusto Tavares Vargas, luizatv@superig.com.br
Bernardo Augusto de O. Vieira, bernardo.augusto@terra.com.br
Center for Aeronautics Studies – Federal University of Minas Gerais

Abstract. *A computer code is currently being developed at the Center for Aeronautic Studies at the Federal University of Minas Gerais (CEA-UFMG) to calculate the aerodynamic characteristics of aircrafts (wings and tails) including non-linear behavior, post-stall and free wake calculations. This code has received the name of CEA-VLM (Vargas e Oliveira, 2006). However, it still cannot estimate the ground effects. In this work, it is presented the process of insertion of this effect to the software CEA-VLM through the implementation of the Three Dimensional Panel Method. The ground is modeled as a non-lifting body, and it is used a constant distribution of sources on each panel. The velocities induced by the sources are calculated based on the geometry of the problem. The influence coefficient matrix is obtained, and it is used to alter the aerodynamic calculation of lifting bodies close to the ground.*

Keywords*: ground effect, vortex-lattice*

1. INTRODUCTION

The aerodynamic design of an aircraft is one of the most important phases of its development. From the conceptual design to the detailed one, the development of the aerodynamic design has major influence on other decisions of the engineering process. The Center for Aeronautic Studies at UFMG, considering its vocation to the development of new aeronautical designs and prototypes, has been developing a new computer code to facilitate the aerodynamic design of its projects. It is a computer implementation of the Vortex-Lattice method with some modifications to consider planar geometries, in a non-symmetric flight condition, and taking into account the non-linear aerodynamic effects of the stall (Vargas, 2006). In order to increase the capabilities of this method, it is presented the implementation process of the effects caused by the ground, called the ground effects.

As mentioned before, the ground effect is noticed when the aircraft is close to the ground. According to Mccormick (1979) and Houghton and Carpenter (2004), the downwash increases as an aircraft approaches the ground. The presence of the ground forces the zero normal force, and consequently modifies the flow behavior around the aircraft. According to Phillips (2004), this phenomenon occurs due to a substantial reduction of the vorticity on the wing trailing edge. Moreover, it is mentioned that the downwash reduction induces an increase on the C_L x alpha curve slope, a reduction of the induced drag, and a change on the neutral points' position. According to Thwaites (1960), the ground induces an upwash on the wing causing a reduction on the induced angle of attack. Therefore, for the same geometric angle of attack, there will be an increase on the lift near the ground. Both authors, Mccormick (1979) and Phillips (2004), present an equation to describe the diminishment of the induced drag due to the ground effect. The procedure used is the same in both cases. The wing is replaced by a single horseshoe vortex and, another horseshoe vortex, with the same intensity but with a different direction of rotation, is reflected in the ground plane (figure 2.1). Therefore, the zero normal force condition is satisfied on the ground plane.

The method presented in this work is a combination of the Vortex-Lattice, to represent the aircraft, and the Panel Method, to represent the ground. The Vortex-Lattice and the Panel Method are briefly described and then it is described the formulation of the ground effect as a combination of these two methods. Results for different wing geometries are presented and compared to results obtained in the literature.

2. PANEL METHOD

The problem to be considered is of an ideal and incompressible fluid which flows in a region *R`* exterior of a boundary surface *S*. The Panel Method proposes a discretization of the body surface in a finite number of panels where it is placed a certain distribution of flow singularities (sources, doublets, vortex, etc). The intensity of these singularities is determined as the boundary conditions are satisfied (ANDERSON, 2001).

The fluid velocities field in any point around a body can be described as the sum of two velocities (Hess and Smith, 1966):

$$\vec{V} = \vec{V}_\infty + \vec{V}_i \tag{1}$$

Where $\vec{V}_\infty$ denotes the non-perturbed flow and $\vec{V}_i$ denotes the velocity induced by the body, in other words, the perturbation in the velocity field due to the surface of the body.

Consider a three-dimensional body divided in N panels (Houghton and Carpenter, 2004). In each panel, it is defined a normal and a tangent unit vector, $\hat{n}_i$ and $\hat{t}_i$, respectively. The velocity induced by a panel *j* at the control point of a panel *i* is defined as $\vec{V}_{ij}$. The components of $\vec{V}_{ij}$ perpendicular and tangential to the surface of the panel *i* can be defined as the scalar product $\vec{V}_{ij} \cdot \hat{n}_i$ and $\vec{V}_{ij} \cdot \hat{t}_i$, respectively. These relations can be described as follow:

$$\begin{aligned} \vec{V}_{ij} \cdot \hat{n}_i &= \sigma_j \left(\vec{V}_{ij(\text{fonte unitária})} \cdot \hat{n}_i \right) \\ \vec{V}_{ij} \cdot \hat{t}_i &= \sigma_j \left(\vec{V}_{ij(\text{fonte unitária})} \cdot \hat{t}_i \right) \end{aligned} \tag{2}$$

Where $\vec{V}_{ij(\text{fonte unitária})}$ denotes the induced velocity at the panel *i* due to a distribution of sources of unit intensity on the panel *j*, and σ_j denotes the intensity of the distribution of sources on the panel *j*. Therefore, the total velocity at the control point *i*, perpendicular to the panel surface, can be described as the sum of the velocities induced by each of the N panels and the free stream velocity:

$$V_{n_i} = \left[\sum_{j=1}^{N} \sigma_j \left(\vec{V}_{ij(\text{fonte unitária})} \cdot \hat{n}_i \right) \right] + \left(\vec{V}_\infty \cdot \hat{n}_i \right) \tag{3}$$

Similarly, for the tangential velocity:

$$V_{t_i} = \left[\sum_{j=1}^{N} \sigma_j \left(\vec{V}_{ij(\text{fonte unitária})} \cdot \hat{t}_i \right) \right] + \left(\vec{V}_\infty \cdot \hat{t}_i \right) \tag{4}$$

The impermeability boundary condition imposes that the normal velocity V_{n_i} must be zero at all *N* panels. Thus, the equation becomes:

$$\left[\sum_{j=1}^{N} \sigma_j \left(\vec{V}_{ij(\text{fonte unitária})} \cdot \hat{n}_i \right) \right] = -\left(\vec{V}_\infty \cdot \hat{n}_i \right) \quad (\text{para } i = 1, 2, ..., N) \tag{5}$$

This equation describes a system of linear algebraic equations. In the matrix form, it becomes:

$$D\sigma = N \tag{6}$$

Where *D* is called influence coefficient matrix, and can be calculated by:

$$D_{ij} = \vec{V}_{ij(\text{fonte unitária})} \cdot \hat{n}_i \tag{7}$$

And N is described by:

$$N_i = -\left(\vec{V}_\infty \cdot \hat{n}_i \right) \tag{8}$$

3. CEA-VLM

The CEA-VLM, as the Vortex-Lattice Method, uses a horseshoe vortex distribution along the wing. At a control point on the wing surface, it is defined a point in which a certain boundary condition will be satisfied. Similarly to the Panel Method, it is created an algebraic equation system in which the variables are the vortex intensities, and the boundary condition defines the right side of the equations. With the calculated vortex intensities, it is possible to calculate the other aerodynamic characteristics of the wing. One of the differences of this method (CEA-VLM) and the others presented in the literature is the way that the horseshoe vortex is placed on the wing surface (Vargas, 2006).

Unlike the Vortex-Lattice Method, the horseshoe vortex distribution occurs only spanwise, with only one vortex along the chord. The horseshoe vortex and the control point are positioned at ¼ and ¾ of the chord, respectively. Thus, it could be said that this method is identical to the one proposed on Weissinger (1947). However, on the software CEA-VLM, the two-dimensional characteristics of the wing airfoil are obtained experimentally (or numerically through an

auxiliary procedure) and they are included on the solution of the problem through an iterative procedure especially developed for this goal (Vargas, 2006). Thus, the post-stall behavior of the wing airfoil is also considered on the aerodynamic calculations, causing the method to become a non-linear method.

Moreover, free wake procedures and induced drag calculation on the Treftz-Plane, allow aircraft calculations in non-symmetric conditions of flight. More detailed information regarding this method can be obtained in Vargas, 2006.

4. GROUND EFFECT IMPLEMENTATION

After briefly describing both methods that will be used, it is necessary to mention how the combination of these methods will occur in order to consider the ground effect on the calculation of the aerodynamics characteristics of lifting bodies. Some considerations have to be made about the compatibility of these methods.

Both methods, the Panel Method and the CEA-VLM, are used to describe an incompressible irrotational flow and, consequently, both satisfy the Laplace Equation. The major difference of these methods is the flow singularity used. In the Panel Method, a constant source distribution is used, and in the CEA-VLM, a horseshoe vortex distribution is used. Thus, the methods are compatible.

To better understand the way of solving the problem, it necessary to observe the Figure 1.

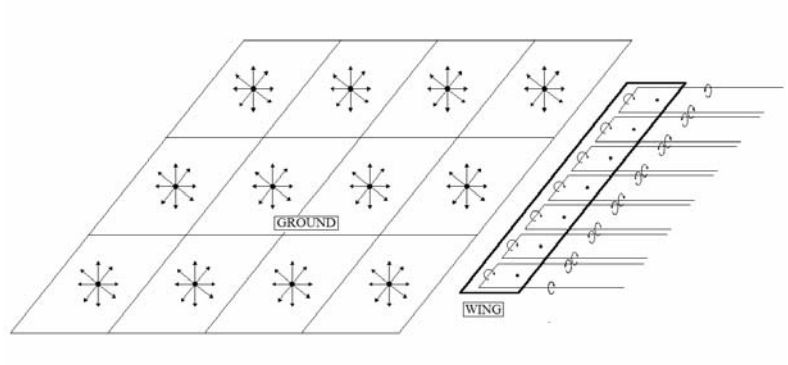

Figure 1 – Simulation Model of the Ground Effect

To solve the flow, it is necessary to consider at each control point, both at the wing and at the ground, the effect of the sources on the ground and the horseshoe vortex on the wing. Then, it is necessary to create a single influence coefficient matrix in which both coefficients due to each singularity are considered. Considering a problem in which the wing is divided in *F* sections and the ground is divided in *N* panels, the following influence coefficient matrix is obtained:

$$D = \begin{pmatrix} b_{11} & b_{12} & \cdots & b_{1F} & c_{1(F+1)} & c_{1(F+2)} & \cdots & c_{1(F+N)} \\ b_{21} & b_{22} & \cdots & b_{2F} & c_{2(F+1)} & c_{2(F+2)} & \cdots & c_{2(F+N)} \\ \vdots & \vdots & \vdots & \vdots & \vdots & \vdots & \vdots & \vdots \\ b_{F1} & b_{F2} & \cdots & b_{FF} & c_{F(F+1)} & c_{F(F+2)} & \cdots & c_{F(F+N)} \\ d_{(F+1)1} & d_{(F+1)2} & \cdots & d_{(F+1)F} & f_{(F+1)(F+1)} & f_{(F+1)(F+2)} & \cdots & f_{(F+1)(F+N)} \\ d_{(F+2)1} & d_{(F+2)2} & \cdots & d_{(F+2)F} & f_{(F+2)(F+1)} & f_{(F+2)(F+2)} & \cdots & f_{(F+2)(F+N)} \\ \vdots & \vdots & \vdots & \vdots & \vdots & \vdots & \vdots & \vdots \\ d_{(F+N)1} & d_{(F+N)2} & \cdots & d_{(F+N)F} & f_{(F+N)(F+1)} & f_{(F+N)(F+2)} & \cdots & f_{(F+N)(F+N)} \end{pmatrix} \tag{9}$$

The coefficients *b* correspond to the influence of the horseshoe vortex on the control points of the lifting surfaces. They represent a matrix of (F x F) elements. The coefficients *c* correspond to the influence of the sources on the control points of the lifting surfaces. They represent a matrix of (F x N) elements. The coefficients *d* correspond to the influence of the horseshoe vortex on the control points of the ground. They represent a matrix of (N x F) elements. The coefficients *f* correspond to the influence of the sources on the control points of the ground. They represent a matrix of (N x N) elements.

The final matrix is a square matrix with (N+F) x (N+F) elements. In a certain element *gij*, the panel *j* induces a velocity on the control point *i*.

To calculate the sources and horseshoe vortex intensities, a consideration has to be made about the matrix N. So, it is necessary to consider the equation that describes the normal induced velocities at each panel:

$$V_{n_i} = \left[\sum_{j=1}^{N} \sigma_j \left(\vec{V}_{ij(\text{fonte unitária})} \cdot \hat{n}_i \right) \right] + \left(\vec{V}_{\infty} \cdot \hat{n}_i \right) \tag{10}$$

Using this equation to the specific case of normal velocity at the wing (control point at the wing):

$$V_{nASA_i} = \left[\sum_{j=1}^{F} \sigma_j \left(\vec{V}_{ij(vortice)} \cdot \hat{n}_i\right)\right] + \left[\sum_{j=F}^{F+N} \sigma_j \left(\vec{V}_{ij(fonte)} \cdot \hat{n}_i\right)\right] + \left(\vec{V}_\infty \cdot \hat{n}_i\right)$$
$$= \left[\sum_{j=1}^{F} \sigma_j \left(b_{ij}\right)\right] + \left[\sum_{j=F}^{F+N} \sigma_j \left(c_{ij}\right)\right] + \left(\vec{V}_\infty \cdot \hat{n}_i\right) \quad (11)$$

Using this equation to the specific case of normal velocity at the ground (control point at the ground):

$$V_{nSOLO_i} = \left[\sum_{j=1}^{F} \sigma_j \left(\vec{V}_{ij(vortice)} \cdot \hat{n}_i\right)\right] + \left[\sum_{j=F}^{F+N} \sigma_j \left(\vec{V}_{ij(fonte)} \cdot \hat{n}_i\right)\right]$$
$$= \left[\sum_{j=1}^{F} \sigma_j \left(d_{ij}\right)\right] + \left[\sum_{j=F}^{F+N} \sigma_j \left(f_{ij}\right)\right] \quad (12)$$

The calculation of the velocity normal to the wing consists of the sum of three terms: the first one indicates the velocities induced by the vortex, the second one indicates the velocities induced by the sources, and the third one indicates the velocity of the free stream. However, in the calculation of the velocity perpendicular to the ground, there are only two terms, as the term due to the free stream should not be included as the ground is parallel to the free stream. Thus, there is not such term on equation (12). Applying the impermeability boundary condition, the matrix used to calculate the intensities becomes:

$$\begin{pmatrix} \sigma_1 \\ \sigma_2 \\ \vdots \\ \sigma_F \\ \sigma_{F+1} \\ \sigma_{F+2} \\ \vdots \\ \sigma_{F+N} \end{pmatrix} = \begin{pmatrix} b_{11} & b_{12} & \cdots & b_{1F} & c_{1(F+1)} & c_{1(F+2)} & \cdots & c_{1(F+N)} \\ b_{21} & b_{22} & \cdots & b_{2F} & c_{2(F+1)} & c_{2(F+2)} & \cdots & c_{2(F+N)} \\ \vdots & \vdots & \vdots & \vdots & \vdots & \vdots & \vdots & \vdots \\ b_{F1} & b_{F2} & \cdots & b_{FF} & c_{F(F+1)} & c_{F(F+2)} & \cdots & c_{F(F+N)} \\ d_{(F+1)1} & d_{(F+1)2} & \cdots & d_{(F+1)F} & f_{(F+1)(F+1)} & f_{(F+1)(F+2)} & \cdots & f_{(F+1)(F+N)} \\ d_{(F+2)1} & d_{(F+2)2} & \cdots & d_{(F+2)F} & f_{(F+2)(F+1)} & f_{(F+2)(F+2)} & \cdots & f_{(F+2)(F+N)} \\ \vdots & \vdots & \vdots & \vdots & \vdots & \vdots & \vdots & \vdots \\ d_{(F+N)1} & d_{(F+N)2} & \cdots & d_{(F+N)F} & f_{(F+N)(F+1)} & f_{(F+N)(F+2)} & \cdots & f_{(F+N)(F+N)} \end{pmatrix}^{-1} \begin{pmatrix} -\vec{V}_\infty \cdot \hat{n}_1 \\ -\vec{V}_\infty \cdot \hat{n}_2 \\ \vdots \\ -\vec{V}_\infty \cdot \hat{n}_F \\ 0 \\ 0 \\ \vdots \\ 0 \end{pmatrix} \quad (13)$$

Where (σ1 .... σF) refer to the horseshoe vortex intensities and (σF+1 .... σF+N) refer to the sources intensities. After calculating the vortex intensities using the equation (13), it is possible to obtain the aerodynamic characteristics of the lifting surfaces (wing or tails), considering the ground effect.

5. RESULTS

After validating the code of the Panel Method through some sphere results, the calculation of the ground effect started. Some modifications had to be done to guarantee that the new geometry, the ground, could be generated. The next step was the insertion of the Panel Method code into the software CEA-VLM (Vargas, 2006). It was necessary to calculate all the influence coefficients that somewhat were related to the ground. These coefficients were previously presented by the letters “c”, “d” e “f” on the matrix (13). To accomplish the calculation of these coefficients, a detailed study of all the CEA-VLM operations was necessary. This study was necessary to prevent any errors in the other operations performed in the software. After a successfully implementation of the Panel Method, the results were generated.

To widely evaluate the ground effect, some wing geometries were defined. They are: i)Rectangular Wing; ii)Trapezoidal Wing with taper ratio 0.6; iii) Rectangular Wing with a dihedral angle of 10º; iv) Rectangular Wing with a sweep angle of 10º. The Figure 2 illustrates the four wings and indicates some of their geometric characteristics.

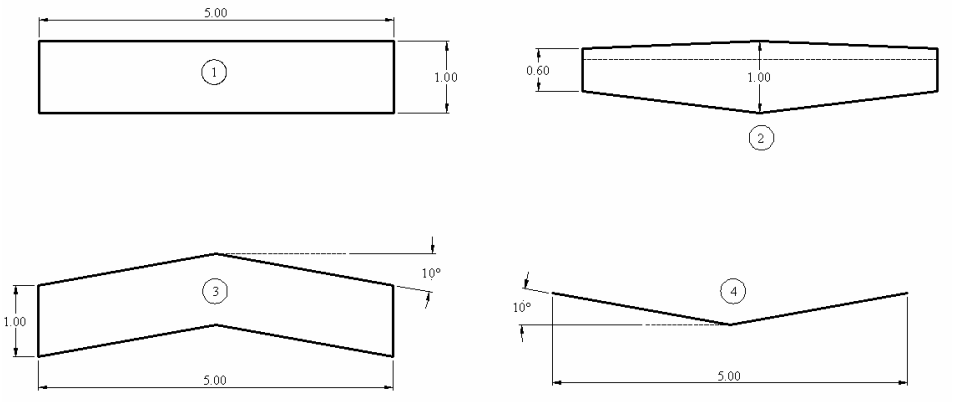

Figure 2 – Wing Geometries

Other relevant parameters of the wings and the flight conditions:

- Wing Airfoil: NACA 0012
- Wing Span (b) = 5m
- Angle of Attack (α) = 5º
- Sideslip Angle = 0º
- Yaw, Pitch and Roll Velocities = All equal zero
- Number of Wing Panels: 20 panels (the convergence of the method is guaranteed with this number of panels)
- Number of Ground Panels: 160 panels.
- Ground Size: Width equal to 2 times the wing span.
  Length before the wing: one wing span.
  Length after the wing: 5 times wing span.

To observe the wing behavior under ground effect, each geometry was tested at different heights (h) above ground: 0.1b, 0.2b, 0.4b, 0.6b, 0.8b, 1.0b, 1.2b, 1.4b, 1.6b, 1.8b, 2.0b, where b represents the wing span. The distance was measured from the wing root of each wing. The ground effect was evaluated through the following variables: i) Global Lift Coefficient of the Wing (CL); ii) Global Drag Coefficient of the Wing (CD); iii) Global Induced Drag Coefficient of the Wing (CDi); iv) Global Parasite Drag Coefficient of the Wing (CDparasita); v) CL/CD Ratio; vi) CL/CDi Ratio; vii) Induced Angle of Attack on each section of the Wing (αi); viii) Lift Distribution on each section of the Wing; v) Induced Drag Distribution in each section of the Wing.

To define the number of panels to be used over the ground, values of convergence were aimed for each case. Next, it is presented the most extreme case for the rectangular wing, which is the calculation of the ground effect at a height of 0.2b. The variable CDi was evaluated because it was the most affected one. Figure 3 shows the values of CDi obtained for many different mesh densities.

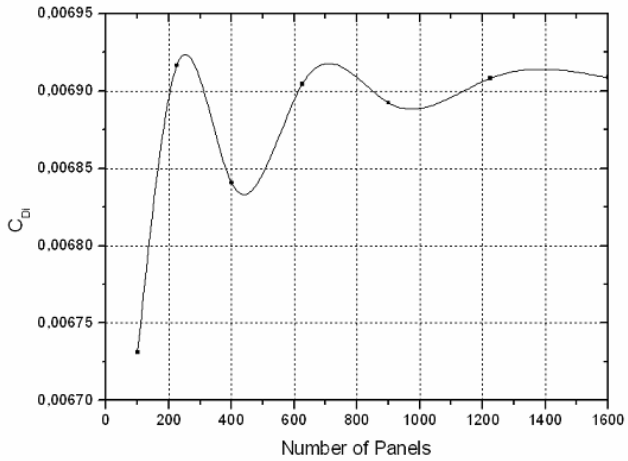

Figure 3 – Convergence of the results for CDi at a height of 0.2b

With a mesh of 1600 panels, the values achieved good convergence with an error of about 0.5%. As the wing gets higher from the ground, the effect reduces; therefore, the number of required panels also reduces. For a distance of 1.0b,

the convergence occurs for 625 panels. All the results were generated considering the required number of panels related to each distance from the ground.

The first variable to be evaluated was the induced angle of attack over ground effect. From a study of the variations of this variable, it becomes easier to understand the aerodynamic consequences of the ground effect. The Figure 4 shows the induced angle of attack distribution spanwise for the four geometries of wings at different heights.

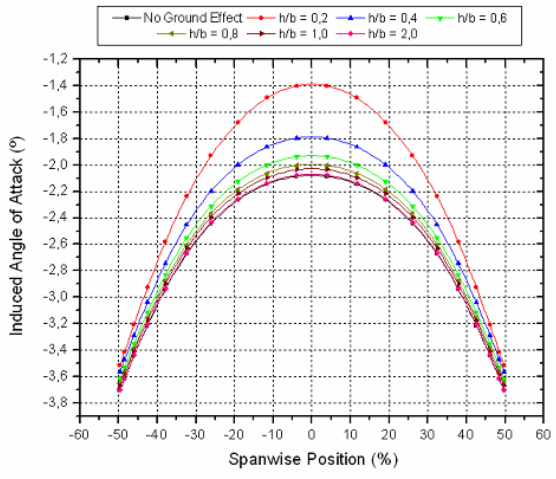

(a) Rectangular Wing

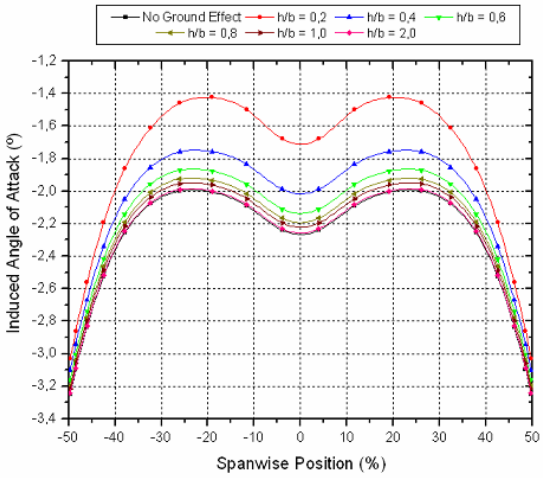

(b) Trapezoidal Wing with Taper Ratio 0.6

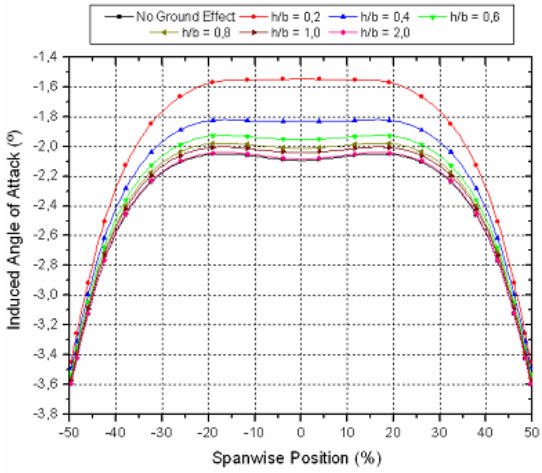

(c) Rectangular Wing with Dihedral Angle of 10º

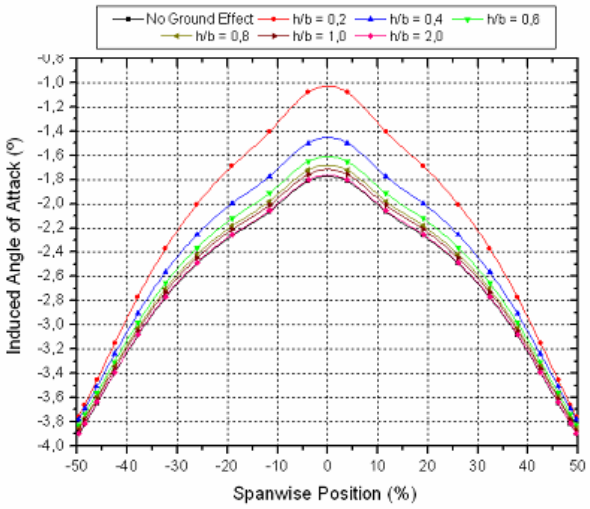

(d) Rectangular Wing with Sweep Angle of 10º

Figure 4 – Induced Angle of Attack Distribution

From these graphics, it is noticeable that in all the wing geometries, a reduction in the induced angle of attack occurs (in modulus); therefore, a reduction in the wing downwash also occurs. This behavior agrees with what is mentioned in the literature. As mentioned before, according to Phillips (2004), the ground effect induces a reduction in the wing downwash, due to a reduction of the vorticity in the wing trailing edge. In other words, it can be said that the sources induce an upwash on the wing, and consequently a reduction on the angle of attack (in modulus).

Observing the curves behavior, it can be noticed that in all wing geometries, the biggest variation of the induced angle of attack takes places at the wing roots. This effect occurs because this region receives the biggest variation of the vortex intensities. These intensities tend to increase as the wing approaches the ground, causing the induced angle to reduce. This diminishment affects the other characteristics of the flow around the wing, such as drag and lift. The Figure 5 compares the numerical results obtained for the drag coefficients. For each wing geometry, the ground effects over the global, induced and parasite drag coefficients are presented. The values in ordinates represents the relation between the drag with ground effect and the drag without ground effect.

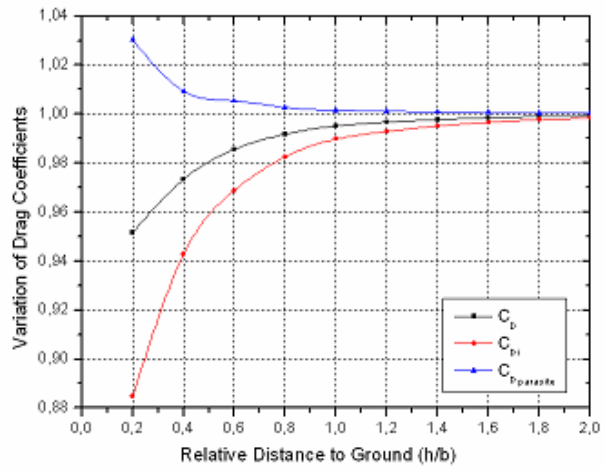

(a) Rectangular Wing

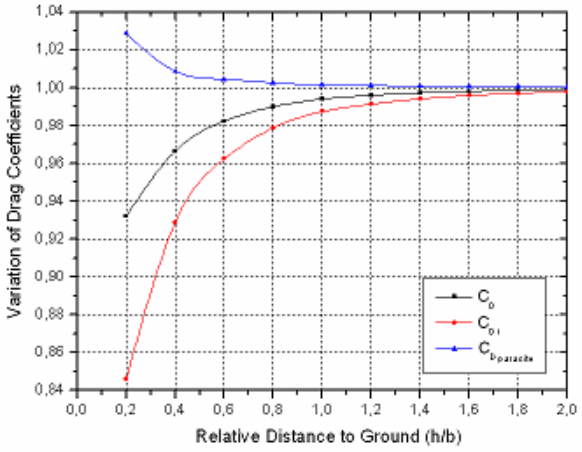

(b) Trapezoidal Wing with Taper Ratio 0.6

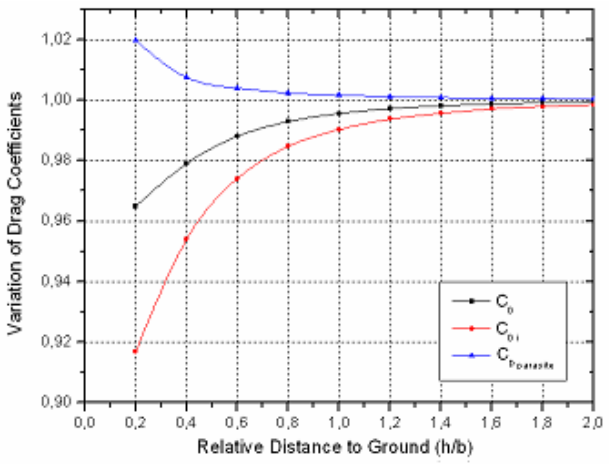

(c) Rectangular Wing with Dihedral Angle of 10º

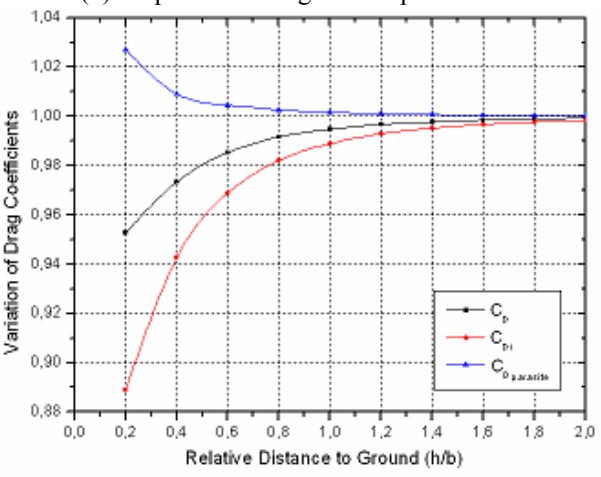

(d) Rectangular Wing with Sweep Angle of 10º

Figure 5 – Drag Coefficients Variation under Ground Effect

From these graphics, it is possible to observe what happens to the components of the global drag coefficients as the wing approaches the ground. In all four geometries, a reduction of the induced drag can be noticed as the wing approaches the ground. This effect was expected as the induced drag is proportional to the induced angle of attack. Moreover, in all cases, there was an increase in the wing parasite drag. The reduction of the downwash over the wing promoted an increase in its effective angle of attack, and consequently an increase on the parasite drag.

Evaluating the global drag, it can be noticed that its values reduces in all tested wings. This fact occurs because the induced drag reduction was higher than the increase of the parasite drag. At a height of 0.2b, the total drag of the rectangular wings reduced around 5%, while the drag of the trapezoidal wing reduced around 7%.

To validate these drag results under ground effect, it was necessary to compare these numerical data with another source of results. The following equation presents an analytical way to calculate the variation that the ground effect causes on the wing induced drag (Mccormick, 1979):

$$\frac{C_{Di}(CES)}{C_{Di}(SES)} = \frac{\left(\frac{16h}{b}\right)^2}{1+\left(\frac{16h}{b}\right)^2} \tag{14}$$

The Figure 6 compares the drag variation obtained by the analytical equation and the numerical results obtained for the four wing geometries.

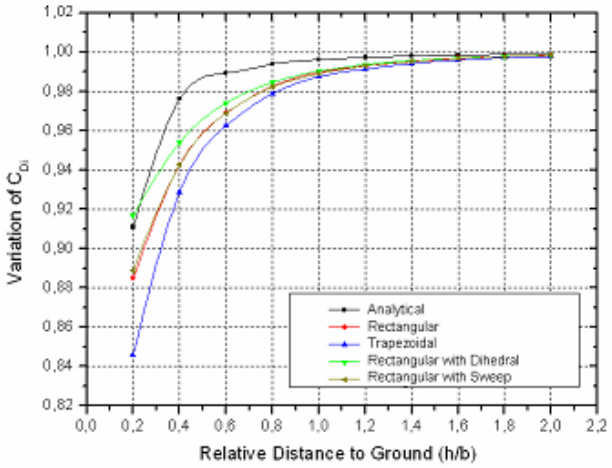

Figure 6 – CDi variation for several heights from the ground

From this figure, it is possible to obtain conclusions of which are the influences of the wing planforms over the CDi results under ground effect. The sweep did not produce any difference on the results, as the rectangular wing and the rectangular wing with sweep curves were practically identical. On the other hand, the trapezoidal wing was the one with the biggest reduction as it approached the ground. At a distance of 0.2b, the CDi reduction was around 15.5%, while on the rectangular one the reduction was around 11.5%. The dihedral rectangular wing, as expected, presented the lowest CDi reduction, because its distances to the ground are higher, especially on the wing tips. This effect is closely related to the dihedral angle.

The analytical values indicate lower reductions of the CDi, in comparison to the numerical values. For a height of 0.6b, the CDi reduced only about 1%. After 0.4b, the ground effect can be better noticed, presenting fast reduction on the induced drag.

Another graphic was necessary in order to compare more clearly the numerical and analytical data. The Figure 7 presents the difference between the analytical and numerical results.

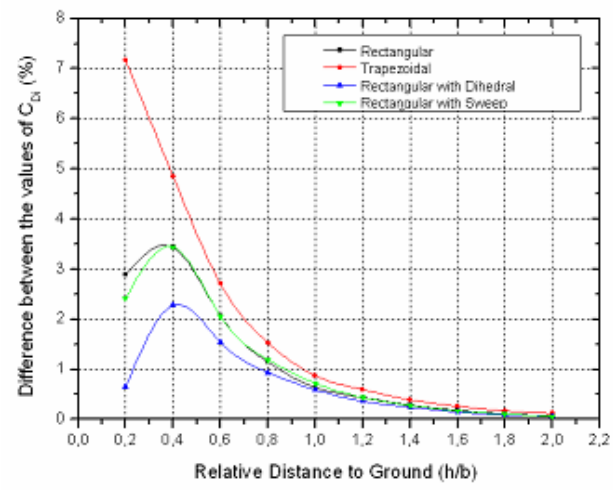

Figure 7 – Difference between the numerical and analytical CDi

From this curve, it is easier to observe the behavior of the numerical curve in relation to the analytical one. For heights of about 1.0b or higher, the differences between the curves do not exceed 1%. However, for closer heights to the ground, the differences become more noticeable, reaching values of about 7% for the trapezoidal wing, at a height of 0.2b. The differences for the rectangular wing are lower, reaching differences of 3.5% at a height of 0.4b. It is not presented in the literature, the validity of the analytical equation for the various planforms. From the results obtained, it can be concluded that, apparently, the analytical equation produces precise data only for simple wing configurations, as the rectangular one.

In spite of the dihedral rectangular wing differences were lower, it cannot be affirmed that the results were more accurate, as the biggest reduction were due to its geometry. This only reinforces that the analytical equation is only valid for rectangular wings. The sweep, as noticed before, practically did not influence the results. Another point that deserves a comment is about the change on the curves behavior at distances closer to the ground than 0.4b. The differences between the curves diminish rapidly due to the fast change of the slope on the analytical curve. Thus, the

analytical curve tends to cross the numerical ones. In this way, the differences tend to reduce as the curves approach one to another.

Figure 8 demonstrate the CL variation for the several planforms tested. The Y-axis presents the ratio of the wing lift coefficient with and without ground effect.

.

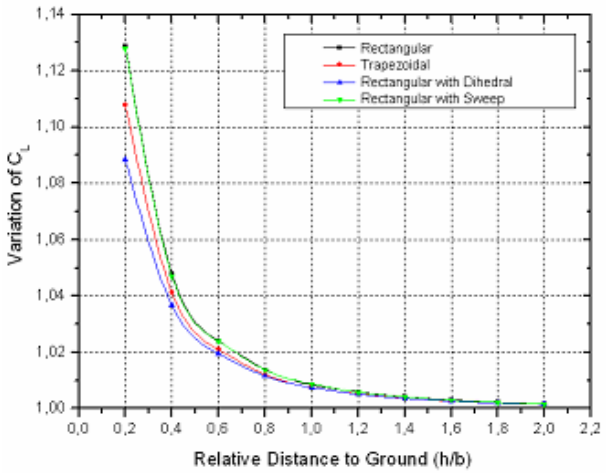

Figure 8 – CL variation for several distances from the ground

The CL variation in function of the height from the ground is approximately the same for all the planforms tested, except for distances very close to the ground. It can be noticed an increase in the CL values, which agrees to what is presented in the literature. According to Thwaites (1960), the increase in the CL is related to the reduction of induced angle, which provokes an increase in the effective angle.

As expected, the dihedral wing responded with less variation on the CL due to the fact that it has higher distances from the ground, in comparison to the others planforms. The reduction was about 9% at a height of 0.2b. The rectangular wing was the most affected by the ground effect, reaching a CL reduction of about 13% at a height of 0.2b. The sweep, one more time, did not cause any relevant variation on the results. The trapezoidal wing presented a CL increase of about 11%.

Through the analysis of the lift and drag coefficient graphics, separately, it is difficult to observe the variation of the CL/CD ratio under ground effect. Thus, a specific graphic should be created, as the one in Figure 9. The Y-Axis presents the ratio of CL/CD with and without the ground effect.

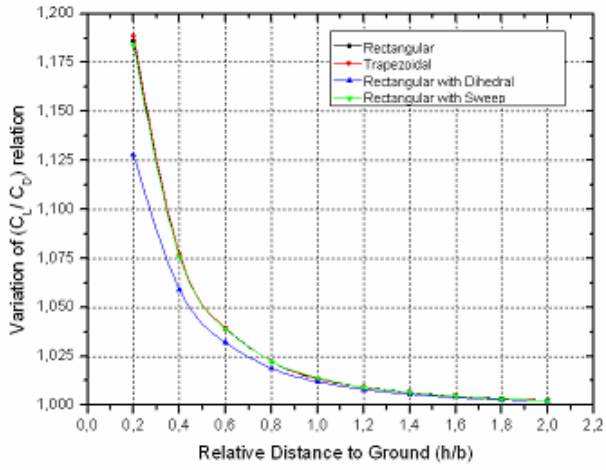

Figure 9 – Variation of the CL / CD ratio as a function of the distance from the ground

This graph shows the CL/CD behavior as the ground effect intensifies. With the exception of the dihedral rectangular wing, in all the other wings, the curve had similar behavior, increasing the same amount. This means that the CL and CD curves of the trapezoidal wing, despite of being different from the others planforms, had compensatory effects that made its CL/CD ratio the same as the other wings. The dihedral wing, one more time, obtained a lower increase due to its geometry.

The Figure 10 shoes the CL/CDi ratio. The Y-Axis, as in the other graphics, presents the ratio of CL/CD with and without the ground effect.

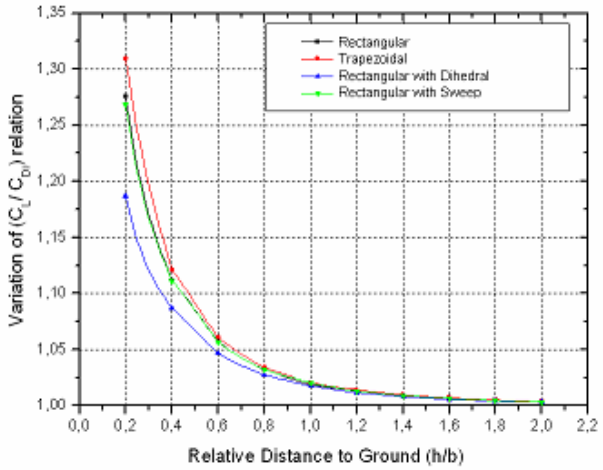

Figure 10 - Variation of the CL / CD ratio as a function of the distance from the ground

As the CDi reduction was lower to all the planforms, the results obtained for the CL/CDi were higher than the ones obtained in Figure 9. The trapezoidal wing obtained values slightly higher than the rectangular wing reaching an increase of about 31% against 28% of the rectangular, for a height of 0.2b.

In order to obtain better signs of the accuracy of the numerical results, it was necessary to calculate values for the relation CDi/CL^2, aiming to compare the results with the ones acquired in a semi-empirical graphic obtained in Hoerner (1965). This semi-empirical graphic presents analytical and experimental data. The figure 11 shows the numerical data and the data obtained in the literature.

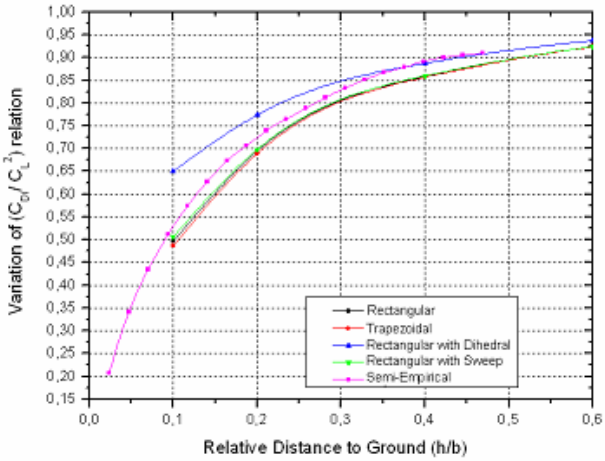

Figure 11 – Comparison between the numerical and semi-empirical data

As it is noticeable, the numerical and semi-empirical curves behaviors are very similar. Only the dihedral wing cannot be compared because the ground effect actuate differently spanwise. For all the other wings, at the height of 0.2b, the difference between the curves is about 4%. At the height of 0.1b, the difference increases to 6%. These values demonstrate that the numerical results obtained were very accurate as, in aerodynamics, results hardly reach this level of precision.

To illustrate, the Figure 12 shows the distribution of source intensities on the ground due to the proximity of different wing shapes.

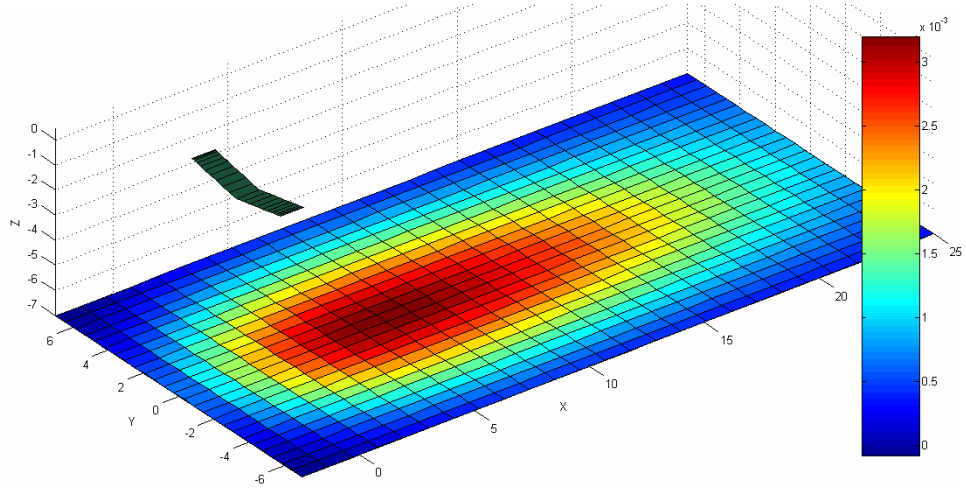

(a) Dihedral Rectangular Wing at a height of 1.4b (7 m)

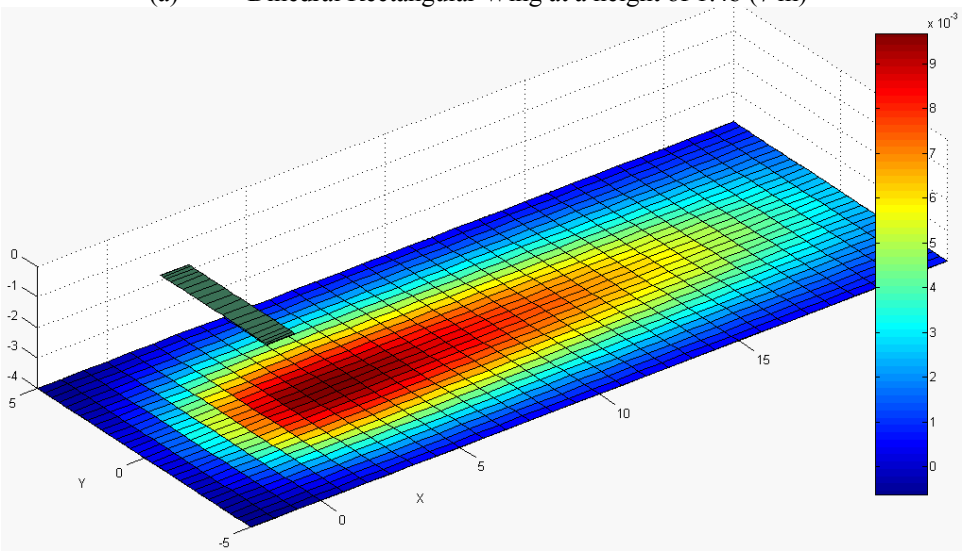

(b) Rectangular Wing at a height of 0.8b (4 m)

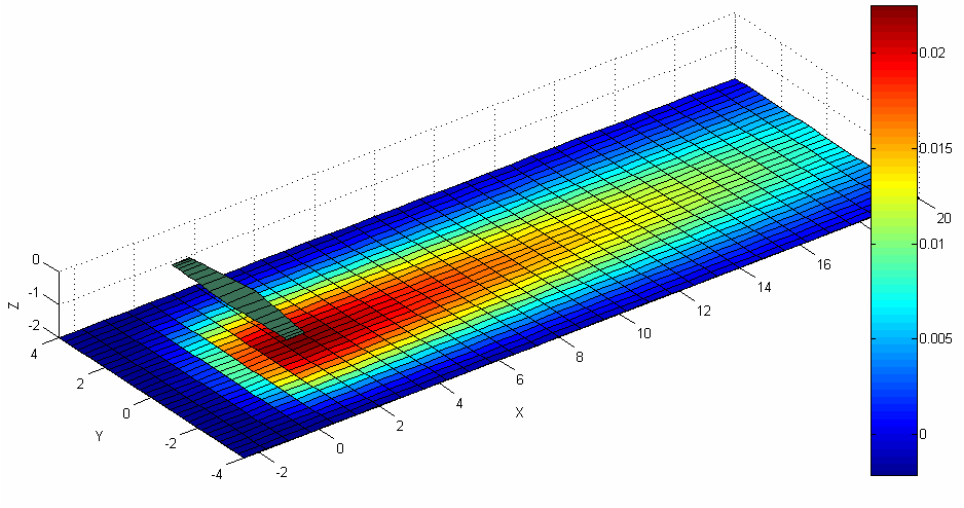

(c) Trapezoidal Wing at a height of 0.4b (2 m)

Figure 12 – Distribution of Source Intensities in several conditions

3. CONCLUSIONS

This paper presents numerical results concern ground effect on the aerodynamics characteristics of finite wings. The results are obtained by the combination of a modified vortex-lattice method, in order to represent the wings, and a panel method, in order to represent the ground.

Several results are presented comparing four different wing geometries in different distances above the ground. These results seem to be precise and suggest that this implementation is correct.

Regardless computational time, no detailed study was performed, but the authors noted that a common case, like these presented in this paper, spend less than one minute to be solved in a personal computer.

Future implementations of this method can include geometries with multiple lifting surfaces and the effect of non-symmetrical conditions of flight such sideslip angles and angular speeds. By this way this method would be a very powerful tool to predict aerodynamics characteristics of airplanes flying near the ground, which is very important information in order to precisely simulate landing and take-off conditions. Additionally, must be noted that normal procedures used to calculate ground effect, like image method, are not able to calculate these further conditions, which makes this method a good choice for a detailed analysis of ground effect.

3. ACKNOWLEDGEMENTS

The authors acknowledge CAPES for financial support.

4. REFERENCES

Anderson Jr., J. D. Fundamentals of Aerodynamics. 3ª.ed. New York: McGraw-Hill Companies, Inc, 2001. 892p.

Hess, J. L. ; Smith, A. M. O. Calculation of Potential Flow About Arbitrary Bodies. Progress in Aeronautical Sciences, New York, Vol. 3, 138p., 1966.

Hoerner, S. F. Fluid Dynamic Drag. Publicação própria; Brick Town; 1965.

Hoghton, E. L.; Carpenter, P.W. Aerodynamics for Engineering Students. 4ª.ed. New Delhi: CBS Publisher & Distributors, 2004. 515p.

Mccormick, B. W. Aerodynamics, Aeronautics and Flight Mechanics. 1ª.ed. New York: John Wiley & Sons, Inc, 1979. 652p.

Phillips W. F. Mechanics of Flight. 1ª.ed. Hoboken: John Wiley & Sons, Inc, 2004. 966p.

Thwaites, B. Incompressible Aerodynamics: An Account of the Theory and Observation of Stead Flow of Incompressible Fluid past Aerofoils, Wings and Other Bodies. Dover Publications, Inc., New York, 1960.

Vargas, L. A. T.; Iscold, P. H. A. O., 2006, A Fast Aerodynamic Procedure for a Complete Aircraft Design Using the Known Airfoil Characteristics" ; SAE Paper 2006-01-2818, Novembro 2006.

Weissinger J. The Lift Distribution of Swept-Back Wing; NACA 1120. Washington: National Advisory Committee For Aeronautics, 1947.

5. RESPONSIBILITY NOTICE

The authors are the only responsible for the printed material included in this paper.